Weak clogging in constricted channel flow

Pascal Viot,* Gregory Page, Chloé Barré, and Julian Talbot†

Laboratoire de Physique Théorique de la Matière Condensée, Sorbonne Université, CNRS UMR 7600, 4, place Jussieu, 75005 Paris, France

(Received 3 September 2021; accepted 16 December 2021; published 11 January 2022)

We investigate simple models of a monodisperse system of soft, frictionless disks flowing through a two-dimensional microchannel in the presence of a single or a double constriction using Brownian dynamics simulation. After a transient time, a stationary state is observed with an increase in particle density before the constriction and a depletion after it. For a constriction width to particle diameter ratio of less than 3, the mean particle velocity is reduced compared to the unimpeded flow and it falls to zero for ratios of less than 1. At low temperatures, the particle mean velocity may vary nonmonotonically with the constriction width. The associated intermittent behavior is due to the formation of small arches of particles with a finite lifetime. The distribution of the interparticle exit times rises rapidly at short times followed by an exponential decay with a large characteristic time, while the cascade size distribution displays prominent peaks for specific cluster sizes. Although the dependence of the mean velocity on the separation of two constrictions is not simple, the mean flow velocity of a system with a single constriction provides an upper envelope for the system with two constrictions. We also examine the orientation of the leading pair of particles in front of the constriction(s). With a single constriction in the intermittent regime, there is a strong preference for the leading pair to be orientated perpendicular to the flow. When two constrictions are present, orientations parallel to the flow are much more likely at the second constriction.

DOI: 10.1103/PhysRevE.105.014604

I. INTRODUCTION

When a stream of moving particles encounters an obstruction, the flow may be reduced, stopped, or intriguingly, made intermittent, i.e., it displays bursts separated by periods of arrest. The outcome depends on a number of factors including, most obviously, the orifice-to-particle size ratio, D/d. Constricted particle flows appear in many diverse situations, including pedestrian and traffic flow in channels [1], silo discharges [2,3], sheep passing through a gate [4], and suspensions of colloidal particles flowing through an obstruction [5,6]. Remarkably, a unified description can be applied to all these situations [7]. An improved understanding of the physics of clogging can be beneficial for real-world applications of granular materials, panic escape [8], microfluidics [9], nanofluidics [10], and efficient methods for single-cell encapsulation [11].

Early studies of the discharge of granular matter from silos showed that significant changes in the flow occur when the ratio of the orifice-to-particle diameter is in the range 3–5 [12]. Later it was realized that the clogging phenomenon is due to the formation of arches spanning the orifice [2,3,13]. The arch stability is normally strongly associated with interparticle frictional forces and is, for example, responsible for the well-known Janssen effect [14–17]. For granular materials, clogging is very often permanent, and an external intervention is required to restore the flow. When friction effects are negligible or entirely absent, the clogging is temporary, leading to intermittent dynamics.

Recent studies have focused on the statistics of blocking processes [5,18,19]. The number of escaping particles in each successive burst, as well as the time intervals between bursts, are distributed exponentially, which implies a constant probability of blocking during the whole burst. The time lapse distribution between successive particles, however, has been shown to exhibit a power-law tail, $p(\tau) \sim \tau^{-\alpha}$ [7]. The transition to clogging is characterized by the divergence of the average time lapse, i.e., $\alpha \leqslant 2$.

Thomas and Durian [20] examined the fraction of grain configurations near the exit of granular hopper flow that cause clogging, and they concluded that there is no sharp transition. Several authors have also studied the strong influence of particle shape on discharge and clogging [21–23]. Colloidal systems, including bacteria [24], involve blocking mechanisms that are governed by, in addition to D/d, the driving force acting on the particles, long-range hydrodynamic interactions, and the nature of the particle-particle and particle-wall interactions. Wioland *et al.* [25] considered geometrically induced turbulence for bacterial mixing processes in microfluidic channels, and Marin *et al.* [5] reported experimental results of clogging in charged-stabilized suspensions of particles flowing through a single constricted channel. The behavior is remarkably similar to that observed in dry granular matter, even though the interparticle interactions are considerably different. For $D/d < 3$, blockages form randomly, while for $D/d > 3$ the flow is uninterrupted. This was attributed to the low friction of the particles. Recently, Souzy *et al.* [6], using a setup similar to that of Marin *et al.* [5] but with a larger constriction angle, observed intermittent flow

*viot@lptmc.jussieu.fr
†talbot@lptmc.jussieu

for $2.43 < D/d < 5.26$ with a power-law exponent $\alpha < 2$ in all cases. Hidalgo *et al.* [26] studied the flow of colloidal suspensions through small orifices using lattice Boltzmann methods with a focus on the effect of varying temperature. They observed that intermittent flow regimes precede clogging events. The mean number of colloids crossing the orifice between clogging events decreased with increasing temperature, i.e., thermal fluctuations can inhibit particle flow through the orifice, an example of "freezing by heating."

Zimmermann *et al.* [27] studied a two-dimensional model of Brownian particles driven through a constriction by an external force using Brownian dynamics simulation and density functional theory. They observed four scenarios: complete blockage, monotonic decay to a constant flux, damped oscillatory, or long-lived stop-and-go behavior.

While most studies of silo discharge involve hard grains, recently soft granular materials have attracted the attention of several researchers [28–34]. A key difference is that, unlike systems with friction, the pressure at the orifice does not saturate as the fill level increases. A striking feature, in comparison with hard grains, is that low-friction soft grains hardly clog even when the orifice is only slightly larger than two particle diameters. These studies also observed the formation of transient clogs.

In this article, we examine the flow characteristics of a monodisperse system of soft, frictionless particles in a narrow channel with a constriction moving under the influence of an external force and the opposing drag exerted by the solvent. Our system is similar to a silo discharging soft particles in that the absence of friction leads to hydrodynamic pressure conditions. We examine the influence of the system parameters, including the channel and constriction geometry, particle stiffness, and temperature, on the flow characteristics. We then focus on those that lead to intermittent flow, which we attempt to characterize. In particular, we examine the interparticle exit time distribution and, where appropriate, the cluster size distribution. We characterize the two-particle metastable arches responsible for the intermittent blocking by examining the orientation of the two leading particles before the constriction.

Many synthetic and natural microchannels have boundaries with a sinusoidally varying, or corrugated, form, e.g., zeolites, microfluidic channels, and nanopores. We therefore extend the model by considering the effect of having two constrictions separated by a fixed distance.

II. MODEL AND SIMULATION

We consider a minimal system, illustrated in Fig. 1, of identical soft disks of mass m and diameter σ_1 flowing through a channel of width L_y. The disks undergo Brownian motion and are driven, from left to right, by the immersing fluid. The moving particles can be deformed by the channel walls or neighboring particles. In many biological situations, deformable molecules move through transport vesicles, which are spherical structures formed by a closed biological membrane, containing molecules and many trans-membrane proteins [35,36]. A constriction formed by two fixed disks of diameter σ_2 is symmetrically placed about the channel axis, at $x = 0$, so that the minimum distance between them is $l_w = L_y + \sigma_1 - \sigma_2$, i.e., they are not centered on the channel

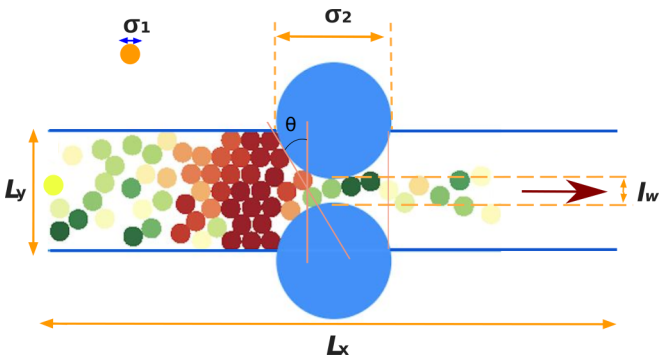

FIG. 1. A channel of width L_y and length L_x contains a constriction formed by two fixed disks, each of diameter σ_2. The orifice width, l_w, is the minimum distance between the obstacles, and σ_1 is the particle diameter. A periodic boundary condition is imposed along the x-axis. The orange vertical represents the abscissa beyond which a particle is considered to have exited the constriction. θ is the angle of the leading pair of particles just before the narrowest part of the constriction.

walls, but displaced outward by $\sigma_1/2$. The channel length L_x is chosen to be significantly greater than L_y in order to minimize correlation effects.

The force between particles i and j is

$$\mathbf{F}_{ij} = k\Theta(\sigma_{ij} - r_{ij})(r_{ij} - \sigma_{ij})\hat{\mathbf{r}}_{ij}, \tag{1}$$

where r_{ij} is the distance between two particles, with unit vector $\hat{\mathbf{r}}_{ij}$. $\Theta(x)$ is the Heaviside function, k is the rigidity factor, and $\sigma_{ij} = \frac{\sigma_i+\sigma_j}{2}$. The same interaction force is used between a mobile particle i and the stationary particles that make up the constriction, i_0.

The force between particle i and the channel walls, denoted $w\pm$, is given by

$$\mathbf{F}_{w\pm,i} = k_w\Theta(r_{iw\pm} - \sigma_1/2)(r_{i,w\pm} - \sigma_1/2)\hat{\mathbf{r}}_{iw\pm}, \tag{2}$$

where $r_{i,w\pm}$ is the distance between the particle i and the wall $w\pm$, $\hat{\mathbf{r}}_{iw\pm}$, the unit vector, and the rigidity factor k_w.

Finally, the moving particles are driven by an external force

$$\mathbf{F}_{d,i} = -\alpha(\mathbf{v} - \mathbf{v}_0), \tag{3}$$

where $\mathbf{v}_0$ is the unimpeded drift velocity along the channel axis, $\mathbf{v}_0 = v_0\mathbf{e}_x$, and α is the drag coefficient.

The system dynamics is described by the overdamped Langevin equation:

$$\mathbf{v}_i(t) = \mathbf{v}_0 + \frac{1}{\alpha}\left(\sum_{j\neq i}\mathbf{F}_{ij} + \sum_{w}\mathbf{F}_{w,i} + \sum_{i_0}\mathbf{F}_{i,i_0}\right) + \sqrt{\frac{2k_BT}{\alpha}}\eta(t), \tag{4}$$

where $\eta(t)$ is a δ-correlated Gaussian noise: $\langle\eta(t)\eta(t')\rangle = \delta(t - t')$.

Further physical parameters characterizing the model are the channel dimensions L_x and L_y. The particle density is $\rho = N/(L_xL_y)$, where the volume occupied by the constriction is neglected. This is reasonable if $L_x \gg L_y$. For the sake of simplicity, we only consider the case in which $k = k_w$. It is convenient to use nondimensionalized quantities. Since, in the

case of the overdamped motion studied here, the particle mass is irrelevant, we select σ_1, σ_1/v_0, and $\sigma_1 v_0 \alpha$ as units of length, time, and energy, respectively. The unit of time corresponds to the ballistic displacement of a particle with the velocity v_0, and the unit of energy is the work done against the drag force in this time. With this choice of units, we introduce the dimensionless quantities

$$k' = \frac{k\sigma_1}{\alpha v_0}, \quad T' = \frac{k_B T}{\alpha v_0 \sigma_1}, \quad \rho' = \rho\sigma_1^2, \tag{5}$$

The channel's reduced geometric parameters are

$$L_x' = \frac{L_x}{\sigma_1}, \quad L_y' = \frac{L_y}{\sigma_1}, \quad l_w' = \frac{l_w}{\sigma_1}, \tag{6}$$

and

$$\mathbf{v}_i'(t) = \frac{\mathbf{v}_i(t)}{v_0}, \quad r_{ij}' = \frac{r_{ij}}{\sigma_1} \tag{7}$$

are the dimensionless velocity and interparticle distance. The Péclet number, giving the ratio of advective transport to diffusive transport, is

$$\mathrm{Pe} = \frac{\sigma_1 v_0 \alpha}{k_b T} = \frac{1}{T'}. \tag{8}$$

In the remainder of the article, we drop the primes for convenience. In a sufficiently long channel, the correlations between exiting and entering particles are negligible. We used $L_x = 60$ in the simulations. Particles are initially randomly and uniformly placed within the channel without overlapping each other, the walls, or the constriction. Periodic boundary conditions are imposed in the direction of the channel, so that as a particle exits $x = L_x/2$, it is reinserted at $x = -L_x/2$. The y-coordinate and velocity of the reentering particle are conserved (randomizing the former within the interval of the channel has no noticeable effect). The average velocity of the system was computed over 20–100 simulations, with a time step of $\delta t = 0.001$, and a total run time of 200.

The next section presents results for a simple convex constriction formed by two fixed large disks located in the middle of the channel (see Fig. 1). In Sec. IV, we consider a double constriction formed by four fixed large disks, whose separation by a finite distance creates a nonconvex region. We focus on the low-temperature regime where the flux displays intermittency, and we monitor the avalanche statistics.

III. SINGLE CONSTRICTION

A. Flow characteristics

Simulations were performed for a reduced density $\rho = 0.55$ and Péclet numbers $1 < \mathrm{Pe} < 100$. This value of the mean density corresponds to $180 < N < 200$ particles for most of the channels studies. After a transient time, which increases as the width of the constriction decreases, the system reaches a stationary state with a well-defined mean particle flux. The upper bound of the time required for the system to reach the stationary state is L_x/v_0, which is equal to the time needed for a particle to traverse the channel. The imposition of constant density (and not number) leads to a roughly constant head of particles before the constriction in the steady state.

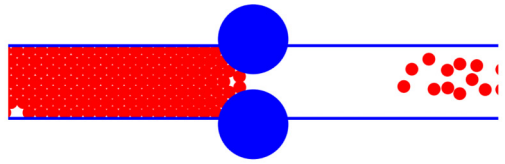

(a) $L_y = 6, l_w = 1.3\ (\sigma_2 = 5.7), T = 0.01$

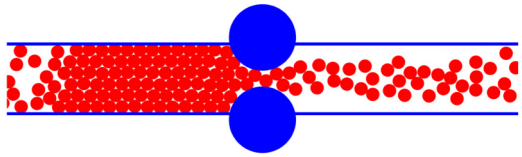

(b) $L_y = 5.5, l_w = 1.8\ (\sigma_2 = 5.2), T = 0.01$

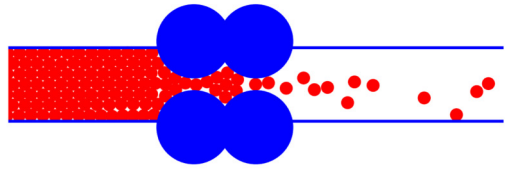

(c) $d_{sep} = 5, L_y = 6, l_w = 1.3\ (\sigma_2 = 5.7), T = 0.05$

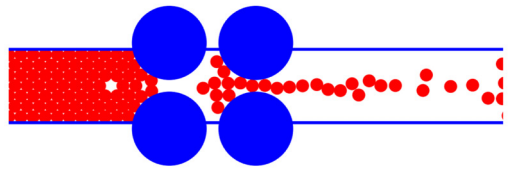

(d) $d_{sep} = 7, L_y = 6, l_w = 1\ (\sigma_2 = 6), T = 0.01$

FIG. 2. Simulation snapshots (cropped). For $L_y = 6$, the particles behind the constriction form a close-packed array of seven layers that is nearly commensurate with the channel width, while for $L_y = 5.5$, six layers at a lower density, and with some defects, are present.

An example of the effect of varying the number of particles at constant density is shown in the Appendix.

In the Supplemental Material (SM), we present five videos to illustrate the behavior of the system: see [37] for mp4 files of the videos. All but one are for $L_y = 6$. With the narrowest constriction, $l_w = 1$, the flow is fairly steady and the particles pass one by one through the constriction. The stream of exiting particles appears to be continuous with no distinct cluster size. The behavior is similar at both temperatures (0.01 and 0.05), but one observes more radial dispersion of the exiting particle stream at the higher temperature.

Increasing the width to $l_w = 1.3$ at $T = 0.01$ leads to a reduced, intermittent flow. Temporary blockages, which result from the formation of a two-particle arch perpendicular to the flow direction, occur frequently. An example is shown in Fig. 2(a). We observe many distinct clusters of 7 (and occasionally 3 and 14) particles in the exiting stream. Let us now compare with an identical system except $L_y = 5.5$. The flow is now continuous and no characteristic clusters are apparent. See Fig. 2(b). At the higher temperature $T = 0.05$

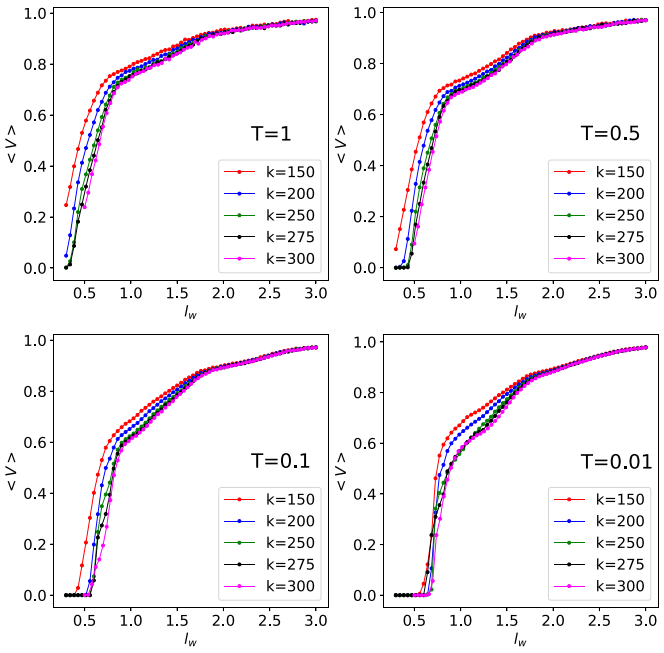

FIG. 3. Mean velocity, $\langle V \rangle$, as a function of the constriction width, l_w, for various rigidities, k, and with $L_y = 5.5$ at different temperatures.

the flow appears much more continuous with only occasional hesitation for both $L_y = 6$ and 5.5.

We now present a quantitative analysis of the flow behavior. We first consider the mean velocity of the system of particles, $\langle V \rangle$, as a function of the minimum distance l_w with $L_y = 5.5$ and for different values of k_w. Figure 3 shows the following behavior, which is repeatedly observed:

(i) For $l_w \geqslant 3$, the constriction has a small effect and the mean velocity remains close to v_0. For $l_{w_1} \leqslant l_w \leqslant 3$, the velocity decreases almost linearly with a slope which increases with decreasing temperature. The lower bound of the linear region, l_{w_1}, depends on the temperature: for $T = 1$ and 0.5, $l_{w_1} \simeq 2$ while for $T = 0.1$ and 0.01, $l_{w_1} \simeq 1.8$. A second regime is observed in the range $l_{w_2} \leqslant l_w \leqslant l_{w_1}$, where l_{w_2} is slightly below 1. The mean velocity is a convex function of l_y and decreases more rapidly than in the previous regimes. The mean velocity depends only weakly on k_w, except at the lowest temperature $T = 0.01$.

(ii) For $l_{w_3} < l_w < l_{w_2}$, which corresponds to a minimum distance less than a particle diameter, the particles pass through the constriction in single file. The velocity decreases rapidly to zero as l_w decreases. The slope of the nearly linear curve increases as the temperature decreases. Moreover, whereas the behavior in this regime depends on the strength of the forces for $T = 1$, 0.5, and 0.1, it is almost independent of k_w at low temperature. l_{w_3} depends on both the temperature and k_w.

(iii) For $l_w < l_{w_3}$, the channel is unequivocally blocked because the force required to sufficiently deform a particle exceeds the force exerted by the other particles behind the constriction.

At low temperatures one observes the formation of a dense region before the constriction in which the particles are almost at rest. When the size of this region exceeds a threshold length, the particles are able to pass through the constriction. The resulting burst is of short duration and followed by a period of arrest before the next release.

Figure 4 shows the mean velocity as a function of l_w for different channel widths L_y. The different regimes described for $L_y = 5.5$ are only slightly modified for $L_y = 4.5$, 6.5, and 7.0. Substantial changes are, however, observed for $L_y = 5$ and 6: For $L_y = 5$, when $l_w \simeq 1.5$, one observes a small dip of the mean velocity, whereas for $1.0 < l_w < 1.5$, the mean velocity decreases slowly with l_w. Finally, a rapid change occurs around $l_w = 1$ where the mean velocity drops to a negligible value if $k_w > 200$. This is because one particle at a time enters the constriction from the dense region before the bottleneck.

When $L_y = 6$, one observes a nonmonotonic variation of the mean velocity, $\langle V \rangle$, with l_w, which is an indication of intermittency. This effect is present for all values of k_w, but the maximum of the depletion/overshoot is obtained for $k_w = 200$. Moreover, for $1.0 < l_w < 1.5$ the minimum of the mean velocity is slightly dependent on k_w. It is worth noting that the convergence of the curves requires a time step $\delta t \leqslant 0.001$. Movies of the simulation (see the SM) suggest that the system now favors two vertically aligned particles at the entrance of the constriction. This configuration is metastable in the sense that, when the fluctuation forces acting on the two particles are sufficiently large, a small deviation of the vertical axis defined by the two particle centers allows one of the two particles to enter the constriction, rapidly followed by the other. This effect only appears if the channel of width L_y is able to "select" this configuration at the entrance of the channel and if the core repulsion is not large (for $k_w = 300$ this same configuration leads to a quasipermanent blockage for $l_w \approx 1.3$, namely larger than a diameter of particle). Conversely, when $k_w = 100$ the particles are highly deformable and the minimum of the mean velocity versus l_w is less pronounced. Thus, for a suitable choice of parameters, metastable minimal arches develop, resulting in blockages of finite duration and particle cascades.

In summary, the mean velocity versus l_w has a roughly similar behavior for different values of the channel L_y, except for $L_y = 6$, where the mean velocity displays a conspicuous, nonmonotonic behavior in the interval of $1 < l_w < 2$. The movies reveal an intermittent regime where two particles located in front of the constriction interrupt the continuous flow. This shows that clogging is possible even for frictionless particles in a confined geometry that selects appropriate configurations of leading particles before the constriction.

B. Detailed analysis of the intermittent regime

To characterize the intermittent regime, we analyze the interparticle time distribution. Each time a particle crosses a line perpendicular to $x^* = \sigma/2$, the time and the particle label are recorded. This choice of abscissa corresponds to a region where a particle is really released. However, because of the stochastic nature of the dynamics, a particle (with a small mean velocity) may cross x^* many times in a short duration (several time steps). Therefore, in order to avoid overcounting the number of exiting particles, only the first

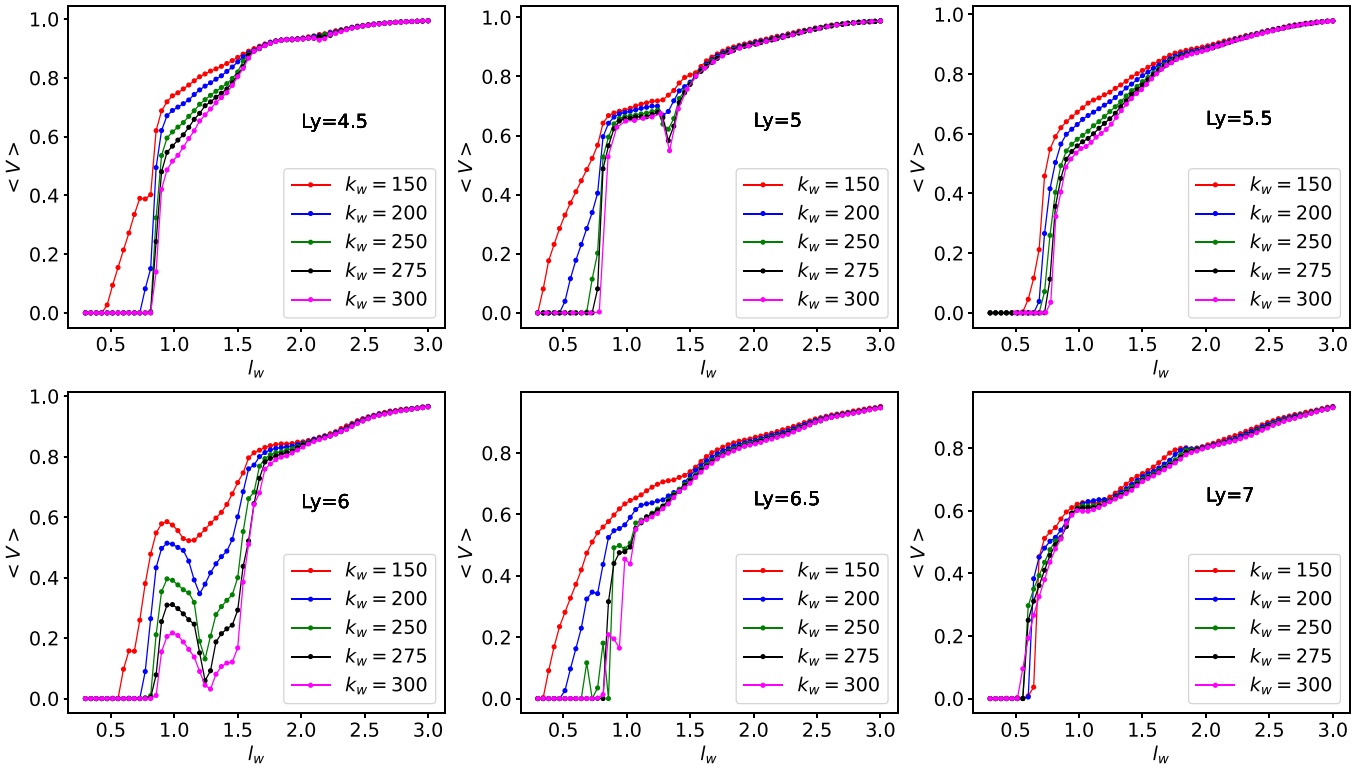

FIG. 4. Mean velocity $\langle V \rangle$ as a function of l_w at low temperature $T = 0.01$, for various rigidities, k_w, and for different values of L_y. A nonmonotonic evolution is observed for $L_y = 6$, and is especially marked for values of rigidity around $k_w = 200$.

crossing is recorded. The time step used was $\delta t = 0.001$. However, to obtain sufficient statistics, the simulation run time was increased to 2×10^4. For this long trajectory we record all times, τ, between two successive particle releases.

Figure 5 displays the interparticle time distribution, $N(\tau)$, for $L_y = 6$, $k_w = 250$, and $\sigma_2 = 5.76$ ($l_w = 1.34$) for which there is a local minimum in the mean velocity at $T = 0.01$ (Fig. 4). A large peak is present at small times in the interparticle time distribution followed by a long tail for $\tau > 1.5$. The first region corresponds to a regular flow of particles through the constriction, whereas the tail corresponds to cascade-associated events. The inset shows a log-log plot of the distribution and the best exponential fit of the tail,

$$N(\tau) \propto e^{-\tau/\tau_0}, \tag{9}$$

where $\tau_0 = 13$ is the typical (mean) interparticle time.

For $T = 0.01$, one observes long interruptions of the flow, corresponding to events when the interparticle exit times are much larger than 1. These events are associated with a typical $\tau_0 = 13$.

For $T = 0.02$ and 0.03, the typical times are reduced by an order of magnitude ($\tau_0 = 1.3$ and 1, respectively). This means that clog duration is significantly shorter than when $T = 0.01$. For $T \geqslant 0.02$, the tail of the interparticle distribution is limited to times less than 10. It is possible to define cascade statistics, but these concern fewer events of shorter duration.

We now examine the cascade size distribution associated with the intermittent regime. Let us define a cutoff time τ_c. A cascade ends if $\tau > \tau_c$ and continues if $\tau < \tau_c$. For example, a cascade of size $n = 3$ occurs if two successive interparticle times are less than τ_c and the following one is greater than τ_c. Once τ_c is set, the trajectory can be viewed as a sequence of cascades, and the cascade intertime distribution, $N(\tau)$, and the cascade size distribution, $D(s)$, can be calculated. An example is shown in Fig. 5.

Unlike the particle intertime distribution, the cluster size distribution is not exponential. Instead, in addition to a small flat background of rare events of all sizes, prominent peaks are present at $s = 3$, 14, and particularly 7 (which can be easily observed in the video). This value corresponds to the release of a hexagonal unit of seven particles. Similarly the peak at 14 corresponds to the successive release of two such units. At the higher temperatures the peaks at $s = 3, 7, 14$ are still present, along with other, emergent peaks in the vicinity of these principal peaks.

The mechanism leading to temporary blockage is illustrated in Fig. 6. When $l_w = 1.3$, the system readily selects configurations featuring a plug of seven particles which is relatively resistant to thermal fluctuations. In contrast, for a narrower constriction, $l_w = 1$, the selected configurations feature a group of eight particles that are much less compact and therefore less stable. This results in a nearly continuous flow.

For reference, we compare the above results with those obtained for $L_y = 5.5$ for which no intermittent regime is observed, Fig. 7. Accordingly, the interparticle exit time never exceeds 1.5, which is consistent with a continuous flow of particles and the absence of distinct clusters.

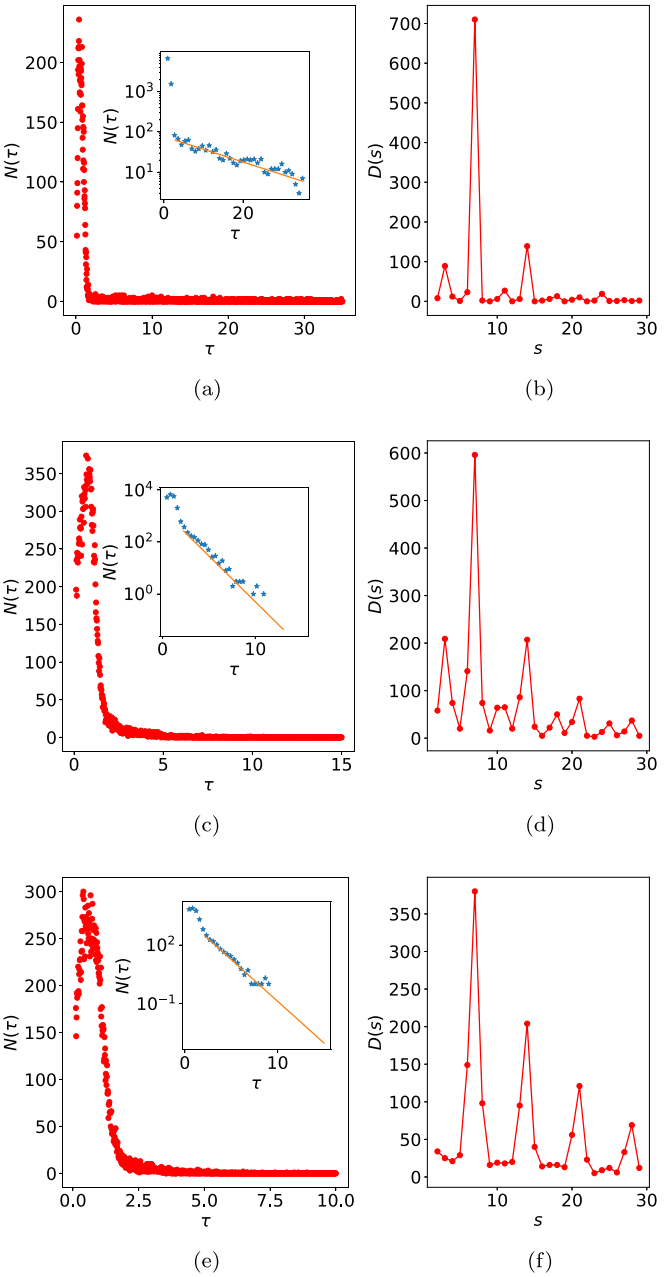

FIG. 5. (a) Interparticle time distribution, $N(\tau)$. The inset displays a semilog plot of $N(\tau)$ and an exponential fit of the distribution. (b) Cascade size distribution. $L_y = 6$, $l_w = 1.24$ ($\sigma_2 = 5.76$), $k_w = 250$, and $T = 0.01$. (c); (d) $T = 0.02$; (e); (f) $T = 0.03$. The exponential fits, Eq. (9), of the particle intertime distributions give the typical times $\tau_0 = 13$, 1.26, and 1.01 for $T = 0.01$, 0.02, and 0.03, respectively.

C. Leading pair orientational distribution

The animations suggest that the intermittent behavior (when present) is due to the formation of metastable, two-particle arches in front of the constriction. We attempted to characterize these arches by examining the orientation of the two leading particles located before the constriction. By monitoring the positions of the leading pair at equal time intervals of $50\delta t$, one builds the probability density function,

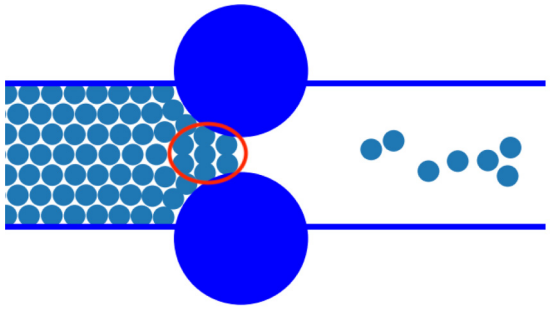

(a) $L_y = 6, l_w = 1.3$ ($\sigma_2 = 5.7$), $T = 0.01$

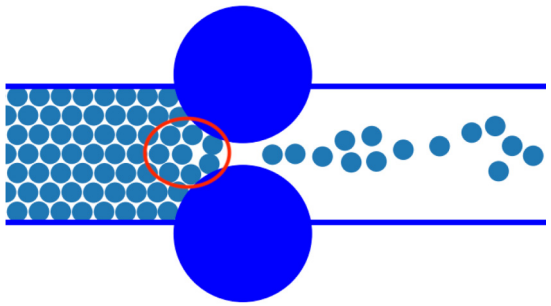

(b) $L_y = 6, l_w = 1$ ($\sigma_2 = 6$), $T = 0.01$

FIG. 6. Simulation snapshots (cropped) showing the blocking mechanism for $L_y = 6$. For clarity the particles are shown 90% actual size. For $l_w = 1.3$, a relatively stable hexagonal plug of seven particles forms leading to a temporary blockage, while for $l_w = 1.0$ the potential plug is composed of eight particles and is much less stable, leading to a nearly continuous flow.

$\Psi(\theta)$, of the angle θ between a line connecting the centers of the leading pair of particles and the y-axis; see Fig. 1. Some examples of the leading pair orientational distribution (LPOD) are shown in Fig. 8, where one observes a trimodal form

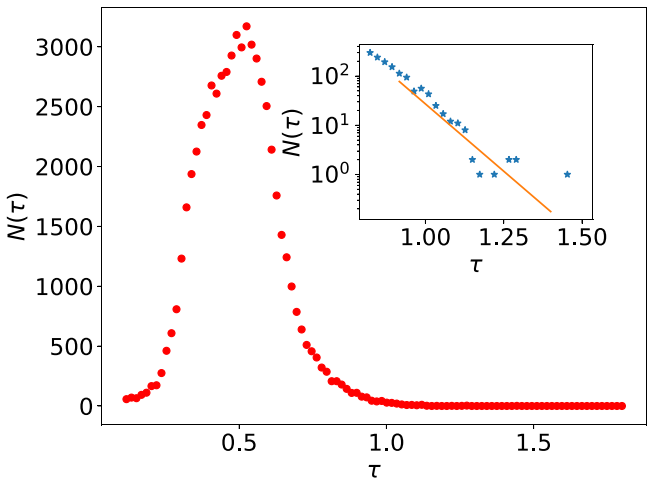

FIG. 7. The interparticle time distribution for $L_y = 5.5$, $l_w = 1.24$ ($\sigma_2 = 5.76$), and $T = 0.01$. In the simulations, the interparticle time never exceeded 1.5, and no cascade distribution can be defined ($\tau_0 = 0.13$).

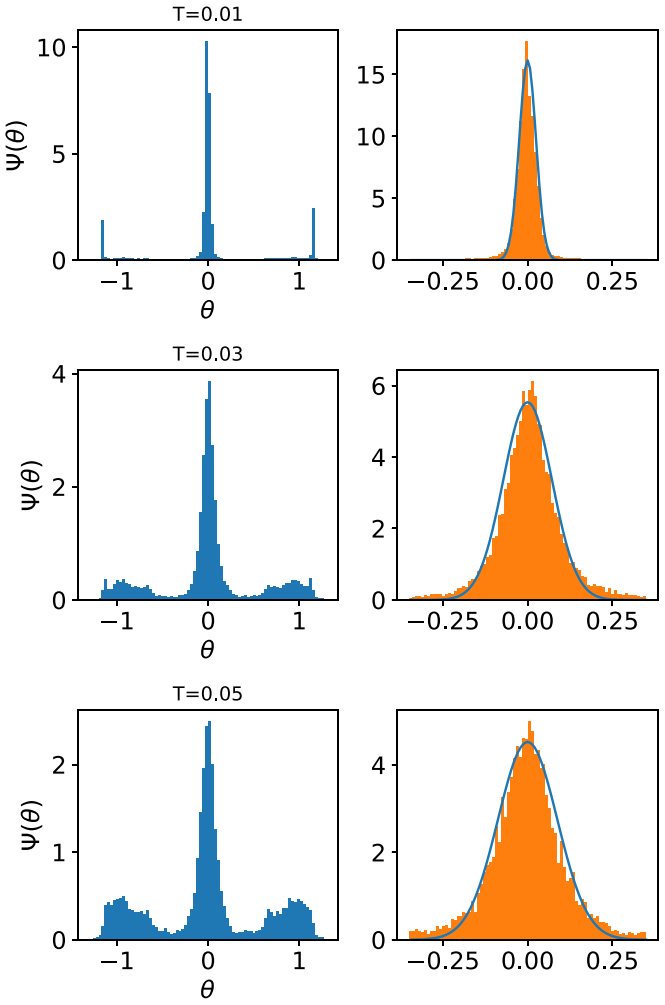

FIG. 8. Left: distribution of the leading pair orientation, θ, for a system with $L_y = 6$, $l_w = 1.25$ ($\sigma_2 = 5.75$) at temperatures $T = 0.01, 0.03$, and 0.05, top to bottom. Right: zoom on the central region of the distribution with the best fits of Eq. (11). The fit parameters are $\alpha T = 4.1$, 1.5, and 1.6 from top to bottom.

with a central peak at $\theta = 0$ that grows as the temperature decreases. This peak corresponds to the situation in which the two particles lie nearly parallel to the y-axis (or perpendicular to the flow direction), which prevents any particle flow. On the other hand, when $|\theta| \approx 1$, the two particles are aligned more parallel to the flow direction and can proceed through the orifice without impediment. More quantitatively, we let

$$\Psi(\theta) = a\Psi_0(\theta) + (1-a)\Psi_1(\theta), \tag{10}$$

where $\Psi_0(\theta)$ and $\Psi_1(\theta)$ are normalized distributions corresponding to the central and outlying peaks, respectively. The area of the central peak, a, then corresponds to the fraction of the total time during which no particle crosses the constriction.

We attempted to fit the central peak $\Psi_0(\theta)$ with the function

$$\Psi_0(\theta) = \frac{e^{\alpha\cos(2\theta)}}{\pi\ I_0(\alpha)}, \tag{11}$$

where $\alpha > 0$ is a fitting parameter and $I_0(\alpha)$ is the modified Bessel function of the first kind, which serves as a normalization factor. The form of Eq. (11) is consistent with the Boltzmann factor $e^{-\beta U(\theta)}$, where $U(\theta)$ is the confining potential and $\beta = 1/k_B T$. For the form chosen, $U(\theta) = U(0) + b\theta^2 + O(\theta^4)$, i.e., a quadratic dependence for small deviations from the vertical direction. The proposed function provides a good description of the central peak, and we note that, except at the lowest temperature $T = 0.01$, the fitting parameter α is inversely proportional to the temperature (see values in the figure caption). The area of the central peaks in Fig. 8, corresponding to the value of a in Eq. (10), evolves smoothly with the temperature: for $T = 0.01$, 0.03, and 0.05, $a = 0.76$, 0,67, and 0.53, respectively. At the lowest temperature of $T = 0.01$, the mean angle of outlying peaks is equal to 1, while at higher temperatures it is close to 0.85.

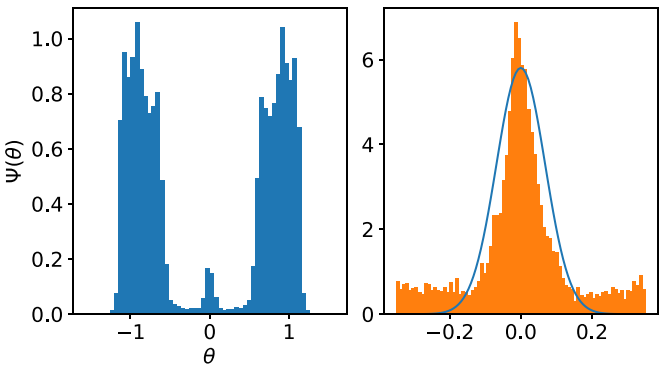

FIG. 9. Left: distribution of the leading pair orientation, θ, for a system with $L_y = 5.5$, $l_w = 1.25$ ($\sigma_2 = 5.25$) at temperatures $T = 0.01$. The weight of the central peak is 3% and the left and the right peaks represent 97% Right: zoom on the central region of the distribution.

When the flow is continuous, the LPOD is quite different. For the system $L_y = 5.5$, $l_w = 1.25$, and $T = 0.01$ shown in Fig. 9, the central peak is barely present, and most leading pairs exit the constriction with an angle in the range $0.87 < \theta < 1.05$.

IV. DOUBLE CONSTRICTION

We now consider the effect of a double constriction consisting of four disks, i.e., the original pair plus a replica displaced by $d_{\rm sep}$. When $d_{\rm sep} = 0$, the two pairs fully overlap and we recover the previous model. When $d_{\rm sep} > 0$, the nonconvex region between the two constrictions may trap the moving particles. Simulations were performed for different values of separation $d_{\rm sep} = \{1, 2, 3, 4, 5, 6, 7, 10\}$. All the other parameters were chosen to correspond to those of the original model ($d_{\rm sep} = 0$) for which both monotonic and nonmonotonic behavior was observed, i.e., for $T = 0.01, 0.05$, $k_w = 200$, and $L_y = 5.5, 6, 6.5$.

Ten videos presented in the SM [37] illustrate the flow characteristics when two constrictions are present (some snapshots are shown in Fig. 2). For $d_{\rm sep} = 3$, $l_w = 1$, and $l_w = 1.3$ the behavior is similar to that observed in the single constriction system: the flow is quite steady, resulting in a continuous stream of particles for $l_w = 1$ and intermittent for $l_w = 1.3$. For the wider orifice, $l_w = 1.5$, we also observe intermittent flow with blockages always forming at the first constriction.

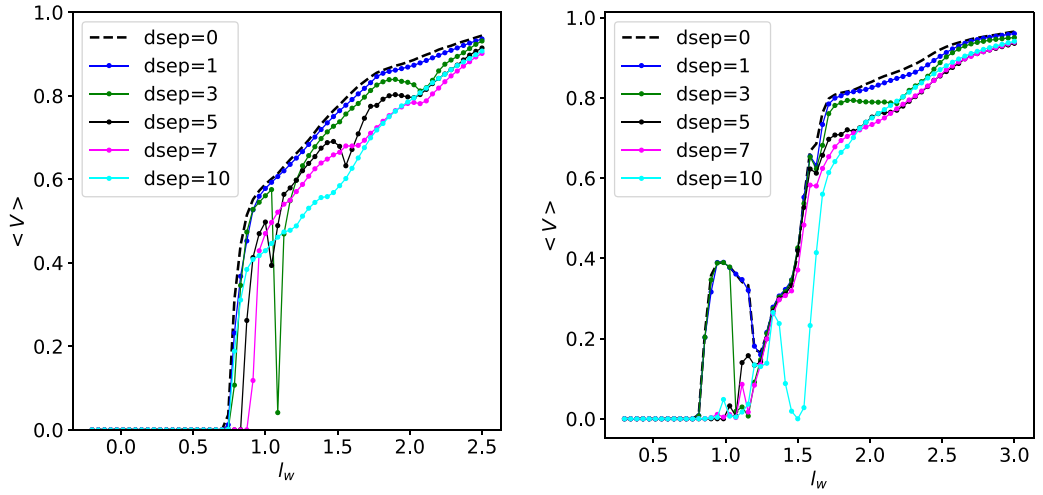

(a) $L_y = 5.5$ (b) $L_y = 6.0$

FIG. 10. Mean velocity $\langle V \rangle$ as a function of l_w for two values of L_y, each for various values of d_{sep} and $T = 0.01$.

For $d_{\text{sep}} = 4$, $l_w = 1.5$, the flow is intermittent. Blockages occur at both obstructions but are more likely to occur at the first one. The pair of particles forming the blocking arch tends to be perpendicular to the flow direction at the first obstacle, while a wider range of leading particle orientations is observed at the second constriction.

For $d_{\text{sep}} = 5$, $l_w = 1$, the flow is stopped for the duration of the video by the second pair of obstacles. The space between the two pairs of obstacles accommodates a group of seven particles in a hexagonal arrangement that forms a stable blockage. The same system at a higher temperature of $T = 0.05$ also forms blockages, but these are more easily destabilized by the larger thermal fluctuations. For the same system but with an orifice width of $l_w = 1.3$ ($T = 0.01$), the flow is intermittent with temporary two-particle arches forming at the first obstacle. The hexagonal group of particles is less easily accommodated in this geometry, and the flow is only slightly impeded by the second constriction.

For $d_{\text{sep}} = 7$, the two constrictions are completely separated. For $l_w = 1$, the flow is initially intermittent, but it is rapidly stopped by a blockage that forms at the second constriction. For the same system at the higher temperature $T = 0.05$ we observe no blockage. Increasing the width to $l_w = 1.5$ results in an intermittent flow with the stream somewhat reduced by the second constriction.

These videos illustrate the complexity of a double constriction system, which results from the interstitial space between the two constrictions, or, in the case of a larger separation, from the possibility of a variation in the number particles before each constriction. Due to this complexity, an exhaustive study of the double constriction system is not feasible. Nevertheless, we present a preliminary quantitative analysis of some systems.

Figure 10 shows the mean velocity as a function of l_w for various values of d_{sep}. As one might expect, the mean velocity is always less than the single constriction system $d_{\text{sep}} = 0$. For small values of d_{sep}, however, it is only marginally smaller for all values of l_w.

Let us consider a channel of width $L_y = 6$. For $l_w > 2$, the mean velocity decreases weakly with increasing d_{sep}, showing that the interconstriction geometry has little influence. In the intermediate range, $0.7 < l_w < 2.0$, the situation is considerably different: for $d_{\text{sep}} = 1, 2$, one observes an overshoot of the mean velocity for $l_w \approx 1$, followed by a minimum comparable to that displayed by the single constriction ($d_{\text{sep}} = 0$).

For larger values, $d_{\text{sep}} = 3, 4$, the minimum of the velocity is much smaller than the previous cases, and it occurs for $l_w = 1.1, 1.3$, respectively. For $d_{\text{sep}} = 5$, the velocity is almost monotonic (except for a tiny plateau in the interval $l_w = [1.0, 1.1]$). The nonmonotonic evolution of the mean velocity, for nonzero values of d_{sep}, persists for cases in which the channel width is noninteger ($L_y = 5.5, 6.0$).

A. Cascade statistics

Figure 11 displays cascade statistics for three different temperatures, for $L_y = 6$, $l_w = 1.27$, $d_{\text{sep}} = 3$, and for $\tau_c = 1$. For this orifice width at $T = 0.01$ the mean velocity is quite low ($\approx$0.1), as shown in Fig. 10. For all temperatures studied, the distributions are nearly exponential, except for a small deviation at $s \approx 12$.

B. Leading pair orientation

We examined the leading pair orientational distribution at both constrictions. Some results are shown in Fig. 12. The distributions before the first constriction are similar to the single constriction case discussed earlier (Fig. 8): they are dominated by a central peak at low temperatures with side peaks that increase with increasing temperature. The LPOD before at the second constriction is, however, quite different. Even at the lowest temperature the side peaks are dominant, and as the temperature increases, the magnitude of the central peak diminishes rapidly. This behavior is consistent with the fact that blockages are much more likely to occur at the first constriction.

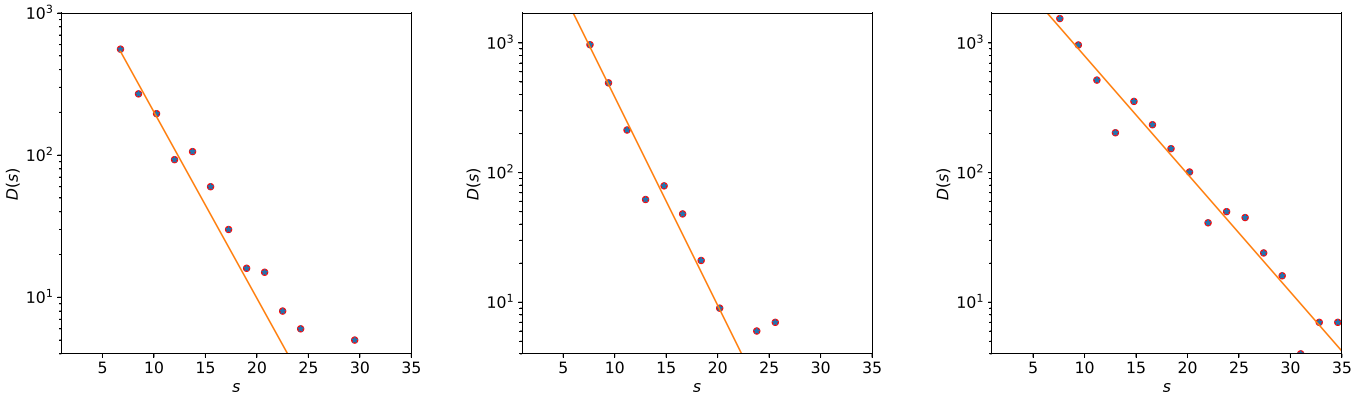

(a) $T = 0.01$ (b) $T = 0.02$ (c) $T = 0.05$

FIG. 11. Cascade size distribution for $l_w = 1.27$ ($\sigma_2 = 5.73$), $L_y = 6$, $d_{\text{sep}} = 3$, $t_c = 1$, for different temperatures T; distribution of cascade sizes, $D(s)$, on a log-linear plot. The exponential fits of the cascade size distribution give the typical size $s_0 = 3.3$, 2.5, and 4.2 for $T = 0.01$, 0.02, and 0.05, respectively.

V. DISCUSSION

We studied the transport of monodisperse, soft, frictionless disks through both a single and a double constriction using overdamped Brownian dynamics simulation. At low temperatures and for certain orifice widths, we observed strongly intermittent dynamics. At low temperatures, the mean velocity varies nonmonotonically with constriction width. As the temperature increases, this behavior diminishes. We performed the simulations at a given mean particle density ($\rho = 0.55$). Since hydrodynamic pressure conditions apply, changing the density will alter the flow characteristics. However, if the density, and hence the head, is sufficiently large, we expect the intermittent behavior will persist.

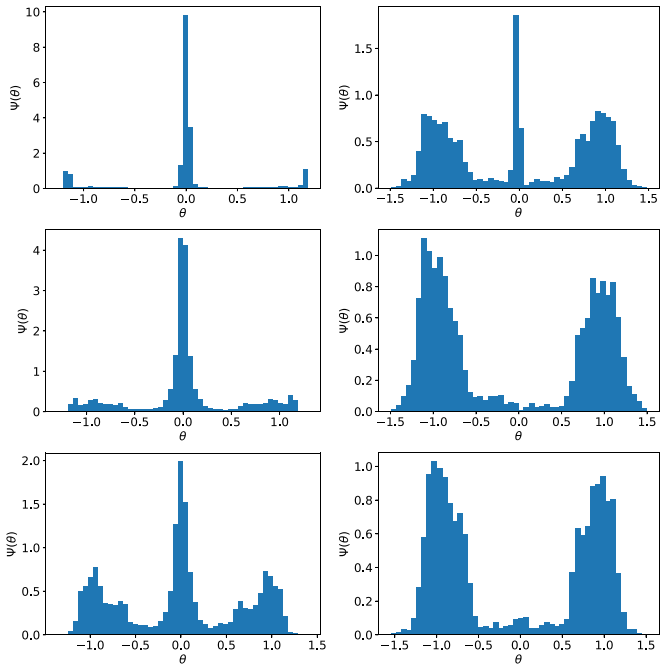

FIG. 12. Leading pair orientational distribution at the first (left) and second (right) constriction for particles flowing through a channel. Parameters correspond to Fig. 11 and $T = 0.01$, 0.02, and 0.05 top to bottom.

The interparticle time distributions are essentially exponential, but the cascade size distributions are not, particularly at low temperatures for which one observes a few strong peaks at distinct cluster sizes corresponding to the release of hexagonal units. Increasing the temperature reduces the cascade size and decreases the interparticle time.

In the presence of a single constriction, the metastable arch is formed by a pair of particles that are strongly aligned perpendicular to the channel axis. Increasing the temperature broadens the central peak of the leading pair orientational distribution while increasing the side peaks.

With two constrictions present, the LPOD at the first constriction is similar to the single constriction case, but an orientation parallel to the flow direction is generally preferred at the second.

While most studies concerning the formation of arches and other blocking phenomena highlight the importance of frictional forces, our results demonstrate that, even in their absence, the degree of confinement strongly influences the formation of arches that lead to intermittent dynamics.

It is interesting to compare our results with the well-known phenomenon in which placing an obstacle upstream from the outlet may reduce or eliminate clogging, e.g., in silos [38], panic escape [8], and even the flow of sheep [39]. In contrast, in the current model, the introduction of the second pair of obstacles increases the likelihood of blockage due to the creation of spaces within which metastable arches may form. Depending on whether the arch formations are desired, knowledge of the relevant parameter range in which they exist would aid any subsequent engineering solution.

The nonequilibrium nature of the process biases the weight of configurations (compared with equilibrium). For a given set of system parameters, these biased configurations may be more or less favorable to the appearance of a temporary blockage. Compared to the silo flow considered by Thomas and Durian [20], the complexity of our model with one constriction may be insufficient to produce a large spectrum of configurations, as illustrated in Fig. 6. With two

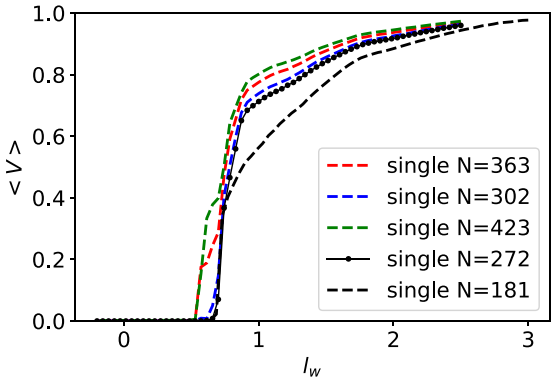

FIG. 13. Mean velocity $\langle V \rangle$ as a function of l_w for different values of N, $L_y = 5.5$, $k_w = 250$, and $T = 0.01$.

constrictions, however, we appear to recover a larger complexity resulting in an exponential decay of the avalanche size distribution.

To obtain additional insight into the phenomena associated with intermittent clogging, it would be useful to examine in detail the mechanism by which the particles pass through the constriction and the stress propagates into the head.

ACKNOWLEDGMENTS

J.T. acknowledges discussions with Tamás Börzsönyi and Ellák Somfai within the framework of the CNRS PICS Grant No. 08187 and the Hungarian Academy of Sciences Grant No. NKM-2018-5. We also thank Éric Clément and Anki Reddy Katha for helpful suggestions.

APPENDIX

We show how the mean flow velocity changes as a function of the number of particles in the system (Fig. 13). Since the particles are frictionless, adding more increases the pressure at the orifice, leading to a larger flow rate.

[1] D. Helbing, L. Buzna, A. Johansson, and T. Werner, Self-organized pedestrian crowd dynamics: Experiments, simulations, and design solutions, Transp. Sci. **39**, 1 (2005).
[2] K. To, P.-Y. Lai, and H. K. Pak, Jamming of Granular Flow in a Two-Dimensional Hopper, Phys. Rev. Lett. **86**, 71 (2001).
[3] A. Janda, I. Zuriguel, A. Garcimartín, and D. Maza, Clogging of granular materials in narrow vertical pipes discharged at constant velocity, Gran. Matter **17**, 545 (2015).
[4] A. Garcimartín, J. M. Pastor, L. M. Ferrer, J. J. Ramos, C. Martín-Gómez, and I. Zuriguel, Flow and clogging of a sheep herd passing through a bottleneck, Phys. Rev. E **91**, 022808 (2015).
[5] A. Marin, H. Lhuissier, M. Rossi, and C. J. Kähler, Clogging in constricted suspension flows, Phys. Rev. E **97**, 021102(R) (2018).
[6] M. Souzy, I. Zuriguel, and A. Marin, Transition from clogging to continuous flow in constricted particle suspensions, Phys. Rev. E **101**, 060901(R) (2020).
[7] I. Zuriguel, D. R. Parisi, R. C. Hidalgo, C. Lozano, A. Janda, P. A. Gago, J. P. Peralta, L. M. Ferrer, L. A. Pugnaloni, E. Clément, D. Maza, I. Pagonabarraga, and A. Garcimartín, Clogging transition of many-particle systems flowing through bottlenecks, Sci. Rep. **4**, 7324 (2014).
[8] H. Dirk, F. Illes, and V. Tamas, Simulating dynamical features of escape panic, Nature (London) **407**, 487 (2000).
[9] E. Dressaire and A. Sauret, Clogging of microfluidic systems, Soft Matter **13**, 37 (2017).
[10] L. Bocquet and E. Charlaix, Nanofluidics, from bulk to interfaces, Chem. Soc. Rev. **39**, 1073 (2010).
[11] M. Sauzade and E. Brouzes, Deterministic trapping, encapsulation and retrieval of single-cells, Lab Chip **17**, 2186 (2017).
[12] W. Beverloo, H. Leniger, and J. van de Velde, The flow of granular solids through orifices, Chem. Eng. Sci. **15**, 260 (1961).
[13] D. Hong and J. McLennan, Molecular dynamics simulations of hard sphere granular particles, Physica A **187**, 159 (1992).
[14] H. A. Janssen, Versuche über Getreidedruck in Silozellen, Z. Ver. Dtsch. Ing. **39**, 1045 (1895).
[15] L. Vanel and E. Clément, Pressure screening and fluctuations at the bottom of a granular column, Eur. Phys. J. B **11**, 525 (1999).
[16] M. Sperl, Experiments on corn pressure in silo cells - translation and comment of janssen's paper from 1895, Gran. Matter **8**, 59 (2006).
[17] S. Mahajan, M. Tennenbaum, S. N. Pathak, D. Baxter, X. Fan, P. Padilla, C. Anderson, A. Fernandez-Nieves, and M. Pica Ciamarra, Reverse Janssen Effect in Narrow Granular Columns, Phys. Rev. Lett. **124**, 128002 (2020).
[18] K. To, Jamming transition in two-dimensional hoppers and silos, Phys. Rev. E **71**, 060301(R) (2005).
[19] I. Zuriguel, A. Garcimartín, D. Maza, L. A. Pugnaloni, and J. M. Pastor, Jamming during the discharge of granular matter from a silo, Phys. Rev. E **71**, 051303 (2005).
[20] C. C. Thomas and D. J. Durian, Fraction of Clogging Configurations Sampled by Granular Hopper Flow, Phys. Rev. Lett. **114**, 178001 (2015).
[21] J. Tang and R. P. Behringer, Orientation, flow, and clogging in a two-dimensional hopper: Ellipses vs. disks, Europhys. Lett. **114**, 34002 (2016).
[22] A. Ashour, S. Wegner, T. Trittel, T. Borzsonyi, and R. Stannarius, Outflow and clogging of shape-anisotropic grains in hoppers with small apertures, Soft Matter **13**, 402 (2017).
[23] A. Hafez, Q. Liu, T. Finkbeiner, R. A. Alouhali, T. E. Moellendick, and J. C. Santamarina, The effect of particle shape on discharge and clogging, Sci. Rep. **11**, 3309 (2021).
[24] E. Altshuler, G. Miño, C. Pérez-Penichet, L. d. Río, A. Lindner, A. Rousselet, and E. Clément, Flow-controlled densification and anomalous dispersion of E. coli through a constriction, Soft Matter **9**, 1864 (2013).
[25] H. Wioland, E. Lushi, and R. E. Goldstein, Directed collective motion of bacteria under channel confinement, New J. Phys. **18**, 075002 (2016).

[26] R. C. Hidalgo, A. Goñi-Arana, A. Hernández-Puerta, and I. Pagonabarraga, Flow of colloidal suspensions through small orifices, Phys. Rev. E **97**, 012611 (2018).

[27] U. Zimmermann, F. Smallenburg, and H. Löwen, Flow of colloidal solids and fluids through constrictions: dynamical density functional theory versus simulation, J. Phys.: Condens. Matter **28**, 244019 (2016).

[28] X. Hong, M. Kohne, M. Morrell, H. Wang, and E. R. Weeks, Clogging of soft particles in two-dimensional hoppers, Phys. Rev. E **96**, 062605 (2017).

[29] A. Ashour, T. Trittel, T. Börzsönyi, and R. Stannarius, Silo outflow of soft frictionless spheres, Phys. Rev. Fluids **2**, 123302 (2017).

[30] R. Stannarius, D. Sancho Martinez, T. Finger, E. Somfai, and T. Börzsönyi, Packing and flow profiles of soft grains in 3d silos reconstructed with x-ray computed tomography, Gran. Matter **21**, 56 (2019).

[31] R. Stannarius, D. S. Martinez, T. Börzsönyi, M. Bieberle, F. Barthel, and U. Hampel, High-speed x-ray tomography of silo discharge, New J. Phys. **21**, 113054 (2019).

[32] K. Harth, J. Wang, T. Börzsönyi, and R. Stannarius, Intermittent flow and transient congestions of soft spheres passing narrow orifices, Soft Matter **16**, 8013 (2020).

[33] T. Pongó, V. Stiga, J. Török, S. Lévay, B. Szabó, R. Stannarius, R. C. Hidalgo, and T. Börzsönyi, Flow in an hourglass: particle friction and stiffness matter, New J. Phys. **23**, 023001 (2021).

[34] R. Tao, M. Wilson, and E. R. Weeks, Soft particle clogging in two-dimensional hoppers, Phys. Rev. E **104**, 044909 (2021).

[35] H. Noguchi, G. Gompper, L. Schmid, A. Wixforth, and T. Franke, Dynamics of fluid vesicles in flow through structured microchannels, Europhys. Lett. **89**, 28002 (2010).

[36] K. Stamer, R. Vogel, E. Thies, E. Mandelkow, and E.-M. Mandelkow, Tau blocks traffic of organelles, neurofilaments, and APP vesicles in neurons and enhances oxidative stress, J. Cell Biol. **156**, 1051 (2002).

[37] See Supplemental Material at http://link.aps.org/supplemental/10.1103/PhysRevE.105.014604 for 15 videos and a commentary.

[38] I. Zuriguel, A. Janda, A. Garcimartin, C. Lozano, R. Arévalo, and D. Maza, Silo Clogging Reduction by the Presence of an Obstacle, Phys. Rev. Lett. **107**, 278001 (2011).

[39] I. Zuriguel, J. Olivares, J. M. Pastor, C. Martín-Gómez, L. M. Ferrer, J. J. Ramos, and A. Garcimartín, Effect of obstacle position in the flow of sheep through a narrow door, Phys. Rev. E **94**, 032302 (2016).